Atmospheric Research 153 (2015) 49–58

Contents lists available at ScienceDirect

Atmospheric Research

journal homepage: www.elsevier.com/locate/atmos

A study of aerosol activation at the cloud edge with high resolution numerical simulations

N. Babkovskaia [a,*], M. Boy [a], S. Smolander [a], S. Romakkaniemi [b], U. Rannik [a], M. Kulmala [a]

[a] University of Helsinki, Department of Physics, Helsinki, Finland
[b] University of Eastern Finland, Department of Applied Physics, Kuopio, Finland

ARTICLE INFO

Article history:
Received 25 November 2013
Received in revised form 30 May 2014
Accepted 16 July 2014
Available online 31 July 2014

Keywords:
Cloud
Aerosol
High resolution numerical simulations

ABSTRACT

High resolution numerical simulations are used to study the structure of the cloud edge area. We consider an aerosol distribution function with a similar aerosol core size (12 nm). The aerosol composition is assumed to be water soluble NaCl. Depending on the specific conditions in the investigated cloud edge area, water is evaporated or activated from the aerosol surface. We use a publicly available high order domain code for direct numerical simulation (DNS) in combination with the Smagorinsky subgrid scale model. We compare 2D and 3D model results of turbulent air motion of aerosol particles with varying grid cell sizes. We show that a 2D model with high resolution gives a more realistic number of activated particles than the corresponding 3D model with lower resolution. We also study the effects of aerosol dynamics on turbulent fields and show that water vapor condensation and evaporation have significant effects on temperature and supersaturation fields.

1. Introduction

Atmospheric aerosol particles affect the Earth's radiative balance both by scattering solar radiation and by acting as cloud condensation nuclei (CCN). CCN are a subset of all the particles that are able to form cloud droplets in atmospheric conditions. The radiative properties of clouds depend on the number of cloud droplets, and an increase in CCN concentration increases the cloud droplet number concentration (CDNC) (Twomey, 1977). A global decrease in CCN by year 2100, resulting from decreased sulfur dioxide emissions, could decrease CDNC by 20% (Makkonen et al., 2012). The change in CDNC, together with decreasing aerosol direct effect due to a decrease in aerosol concentration, would change the aerosol total forcing from present day to year 2100 by up to 1.4 W m^{-2} (Makkonen et al., 2012).

CDNC does not depend on the activation at cloud base in any simple manner, but the cloud is a dynamic system with spatially and temporally varying properties. More cloud droplets may form due to in-cloud activation, and entrainment of air from cloud edges may lead to formation of fresh cloud droplets (Brenguier and Grabowski, 1993; Wyszogrodzki et al., 2011; Slawinska et al., 2012). On the other hand, mixing at cloud boundaries, or in-cloud dynamics, can cause part of droplets to evaporate (Wood et al., 2002; Romakkaniemi et al., 2009; Morales et al., 2011).

In-cloud dynamics can be important especially in stratus type clouds with long in-cloud residence time of air parcels. Mixing at cloud boundaries takes place in all clouds, and the type of mixing depends on the conditions and mixing time scales. In homogeneous mixing, all droplets lose water but their number concentration is not affected. In heterogeneous mixing, a fraction of the droplet population experiences evaporation and forms aerosol particles with size much smaller than the size of prevailing cloud droplets. Depending on the time scales, the moisture content of entraining air, and the size of droplets, either homogeneous or heterogeneous mixing can be dominating (Andrejczuk et al., 2009).

Different phenomena related to aerosol cloud interactions and cloud dynamics involve a large range of scales. Microphysics of cloud–aerosol interactions can be studied by process models,

* Corresponding author.
E-mail address: NBabkovskaia@gmail.com (N. Babkovskaia).

http://dx.doi.org/10.1016/j.atmosres.2014.07.017
0169-8095/

or so called box models, which are mainly used to study how and which aerosol particles are able to form cloud droplets. At the other end of the scale are global models, which are needed to assess how changes in cloud properties affect the global radiation budget. Between these scales there are cloud resolving model (CRM) or large eddy simulation (LES) model that can be used to study cloud dynamics and for example the effect of aerosol on drizzle formation. However, even in CRM the scale (resolution > 1 m) is such that subgrid-scale turbulence needs to be parameterized. One of the methods to provide these parameterizations is direct numerical simulation (DNS) which can be used to study for example cloud boundaries up to a scale of few meters, or few tens of meters (e.g. (Mellado, 2010; Lanotte et al., 2009; Kumar et al., 2013)).

In previous studies, direct numerical simulations have been used to model microscale cloud–clear air mixing (Andrejczuk et al., 2004, 2006). The model physics was based on the Boussinesq approximation: density, kinematic viscosity, and the molecular diffusivity of the temperature and water vapor are assumed to be constant. The temperature evolution is determined by the thermal flux and by the release/absorption of the energy due to evaporation/condensation of/on water droplets. Additionally, they ignore the solute effect (Seinfeld and Pandis, 2006) and consider 16 size classes of the cloud droplets, with droplet sizes linearly distributed from 0.78 to 24 μm.

Comparing these earlier studies on aerosol cloud formation processes with the new model in this paper, the most important differences are: the gas is compressible; thermal conductivity and diffusion coefficients of every species and of a mixture are not constant and are described by the accurate expressions (Babkovskaia et al., 2011); thermal flux, change of energy by evaporation/condensation and viscous heating are included in the energy equation; and the solute effect is taken into account. To study the activation of aerosol particles we take 80 classes of the cloud droplets with the droplet size logarithmically distributed from 80 nm to 10 μm. We take the grid sizes of 0.5 cm, 1 cm, 2 cm, and 4 cm. Since the considered grid sizes are larger than the estimated Kolmogorov scale of $O(1)$ mm, we use the Smagorinsky subgrid scale model with parameter $C_s = 0.15$ for turbulent viscosity (Andrejczuk et al., 2004; Haugen and Brandenburg, 2006).

This paper is organized as follows. A detailed description of the model is presented in Section 2. Section 3.1 presents a 1D model to study aerosol evaporation/condensation (further we use *aerosol dynamics*) in a cloud edge area in a laminar regime. Sections 3.2–3.4 present results from 2D and 3D models with different resolutions. The main objective of this study is two-fold: to test the importance of the model resolution and to compare 2D and 3D model runs for correct simulations of aerosol activation. In Section 3.5 we study the effect of turbulent motion on aerosol dynamics. In Section 4 we will provide our conclusions.

2. Methods

We use the open source PENCIL code, which implements a high order finite difference method for compressible hydrodynamic flows. The code is highly modular and comes with a large selection of physics modules. It is widely documented in the literature and has been used for many different applications ((Dobler et al., 2006; The PENCIL Code, 2001), and references therein). Recently, a detailed chemistry module has been implemented, including an accurate description of all necessary quantities, such as diffusion coefficients, thermal conductivity, and reaction rates (Babkovskaia et al., 2011). This module was well tested by using a commercial code (Chemkin) for calculations of a turbulent combustion process. Our new aerosol module, coupled to the PENCIL Code, is now prepared for calculating condensation dynamics of aerosol particles. In the simulations, the composition of the aerosol cores is assumed to be NaCl which is a soluble aerosol and will dilute inside the droplets.

Originally, the PENCIL Code was developed for studying turbulent motions, so it is well suited for modeling the fluid mechanical processes in atmospheric clouds. Additionally, due to an accurate description of the chemistry, the PENCIL Code is a powerful tool for studying the aerosol dynamics in a turbulent medium with complicated chemical composition. The scientific goal for the construction of the new model is to investigate the spatial distribution of aerosol particles, turbulent mixing of clouds with the environment and the influence of turbulence on aerosol dynamics (and vice versa).

2.1. Fluid dynamic equations

The continuity equation is solved in the form

$$\frac{\mathrm{D}\ln\rho}{\mathrm{D}t} = -\nabla\cdot\boldsymbol{U}, \tag{1}$$

where $\mathrm{D}/\mathrm{D}t = \partial/\partial t + \boldsymbol{U}\cdot\nabla$ is the advective derivative, ρ is density, and $\boldsymbol{U}$ is velocity.

The momentum equation is written in the form

$$\frac{\mathrm{D}\boldsymbol{U}}{\mathrm{D}t} = \frac{1}{\rho}(-\nabla p + \boldsymbol{F}_{\mathrm{vis}}) + \boldsymbol{k}B, \tag{2}$$

where p is pressure, $\boldsymbol{k}$ is the unit vector in the vertical, B is buoyancy, and

$$\boldsymbol{F}_{\mathrm{vis}} = \nabla\cdot(2\rho\nu_t\boldsymbol{S}) \tag{3}$$

is the viscous force, where $\boldsymbol{S}_{ij} = \frac{1}{2}\left(\partial\boldsymbol{U}_i/\partial x_j + \partial\boldsymbol{U}_j/\partial x_i\right) - \frac{1}{3}\delta_{ij}\nabla\cdot\boldsymbol{U}$ is the traceless rate of strain tensor, and ν_t is turbulent viscosity. Following Haugen and Brandenburg (2006), in Smagorinsky model we use $\nu_t = (C_s\Delta)^2\sqrt{2\boldsymbol{S}^2}$, where Δ is the filter size which is equivalent to the mesh size.

The equation for the mass fractions of each species (except water vapor) is

$$\rho\frac{\mathrm{D}Y_k}{\mathrm{D}t} = -\nabla\cdot\boldsymbol{J}_k, \tag{4}$$

where $Y_k = \rho_k/\rho$ is the mass fraction, ρ_k is the density of kth component, and $\boldsymbol{J}_k$ is the diffusive flux for species k. For water vapor we have

$$\rho\frac{\mathrm{D}Y_{wk}}{\mathrm{D}t} = -\nabla\cdot\boldsymbol{J}_{wk} - \rho C_d, \tag{5}$$

where C_d is the condensation rate.

Finally, the energy equation is

$$\left(c_p-\frac{R}{m}\right)\frac{\mathrm{D}\ln T}{\mathrm{D}t}=\sum_k\left(\frac{h_k}{T}-\frac{R}{m_k}\right)\frac{\nabla\cdot\boldsymbol{J}_k}{\rho}-\frac{R}{m}\nabla\cdot\boldsymbol{U}+\frac{2\nu_t\boldsymbol{S}^2}{T}-\frac{\nabla\cdot\boldsymbol{q}}{\rho T}+\left(c_p-\frac{R}{m}\right)\frac{LC_d}{c_pT}, \tag{6}$$

where T is temperature, c_p is heat capacity at constant pressure, R is the universal gas constant, h is enthalpy, m_k is molar mass of the kth species, m is the molar mass of the mixture, $\boldsymbol{q}$ is the heat flux (see details in Babkovskaia et al. (2011)), and $L=2.5\times10^6\ \mathrm{J\,kg^{-1}}$ is the latent heat of condensation for water.

The reason for solving for the temperature directly, instead of e.g. the total energy, is to avoid finding the temperature from the total energy afterwards. In this work we use the ideal gas equation of state given by

$$p=\frac{\rho RT}{m}. \tag{7}$$

2.2. Evolution of the number density function

The equation for the evolution of the number density function takes the form (Mattila et al., 1997; Andrejczuk et al., 2004)

$$\frac{\mathrm{D}^*f}{\mathrm{D}^*t}=-\frac{\partial}{\partial r}\left[f\frac{dr}{dt}\right] \tag{8}$$

$$\frac{dr}{dt}=\frac{\mathrm{D}_w m_w}{RT\rho_w}\frac{(p_v-p_{vs})}{r} \tag{9}$$

where $f(\boldsymbol{x}, r_0, r, t)dr$ is the number of cloud droplets, with the solid core of the size r_0 (covered by the liquid water) and radius between r and $r+dr$, in a unit mass of air about a given point $(\boldsymbol{x}, t)$ in space and time. $\mathrm{D}^*/\mathrm{D}^*t=\partial/\partial t+(\boldsymbol{U}-\boldsymbol{k}v_t)\cdot\nabla$ is the derivative along a droplet trajectory, dr/dt is the particle growth rate, D_w is the water diffusion coefficient (Hirschfelder et al., 1969), and m_w is water molecular mass. According to the Stokes law, $v_t(r)=Cr^2$ is the sedimentation velocity, where constant C is selected to satisfy $v_t(r=10\ \mu\mathrm{m})=10^{-2}\ \mathrm{m\ s^{-1}}$.

Water vapor pressure over a droplet of radius r is defined as (Seinfeld and Pandis, 2006)

$$p_{\mathrm{vis}}=p_0\exp\left(\frac{A}{2r}-\frac{B(r_0)}{8r^3}\right) \tag{10}$$

where p_0 is the water vapor pressure over a flat surface (see Table 1) at the same temperature, $A=0.66/T$ (in μm), and

$$B(r_0)=2\times10^{-17}\left(\frac{r_0}{1.2\times10^{-6}}\right)^3, \tag{11}$$

where r_0 is the radius of the droplet core.

In a general case, the number density function $f(\mathbf{x}, M_s, r, t)$ is a function of the solute mass per particle M_s and the size of the particle r. We ignore the dependence on M_s and assume that all particles have the same solute mass which does not change with time. Therefore, $B(r_0)\simeq 34.4\nu M_s/m_s\ \mathrm{cm^3}$ is a constant,

Table 1
p_0 is water vapor pressure over a flat surface in bar, and T is temperature in °C (Seinfeld and Pandis, 2006).

	$p_0=a_0+a_1T+a_2T^2+a_3T^3+a_4T^4+a_5T^5+a_6T^6$
a_0	6.107799961
a_1	4.43651852110^{-1}
a_2	1.42894580510^{-2}
a_3	2.65064847110^{-4}
a_4	3.03124039610^{-6}
a_5	2.03408094810^{-8}
a_6	6.13682092910^{-11}

where (for example, for NaCl) $m_s=58.5\ \mathrm{g\ mol^{-1}}$ is the solute molecular weight, and $\nu=2$ is the number of ions resulting from the dissociation of one solute molecule (Seinfeld and Pandis, 2006). In all further calculations $B(r_0)=2\times10^{-17}\ \mathrm{cm^3}$ is taken to be a parameter.

The condensation rate derives from the growth of cloud droplets

$$C_d=12\pi\rho_w\rho\int fr\mathrm{D}_w\left(Y_{\mathrm{H_2O}}-Y_{vs}\right)dr, \tag{12}$$

where $Y_{vs}=p_{vs}/(RT)\rho$ is the saturated water vapor mass fraction and $Y_{\mathrm{H_2O}}=p_v/(RT)\rho$ is the water vapor mass fraction, where $p_v=pm/m_vY_{\mathrm{H_2O}}$ is water vapor pressure, and m_v is water molar mass.

2.3. Buoyancy

Buoyancy is defined as (Andrejczuk et al., 2004)

$$B=g\left[\frac{T-T_0}{T_0}+\epsilon\left(Y_{\mathrm{H_2O}}-Y^0_{\mathrm{H_2O}}\right)-Y_c\right], \tag{13}$$

where $g=9.81\ \mathrm{m\ s^{-2}}$ is the acceleration of gravity, $T_0=293\ \mathrm{K}$ and $Y^0_{\mathrm{H_2O}}=9.9\ \mathrm{g\ kg^{-1}}$ are the reference temperature and water vapor mass fraction, $\epsilon+1=R_v/R_d$ is the ratio of the gas content for water vapor and dry air, and the cloud water mixing ratio Y_c is defined as

$$Y_c=\frac{4\pi\rho_w}{3}\int fr^3dr. \tag{14}$$

2.4. Initial and boundary conditions

The purposes of this paper are to analyze the importance of the resolution of the calculation domain and check the validity of the 2D approach for studying the aerosol activation. Since the presented analysis is mostly qualitative, for our simulations we take parameters which are typical for atmospheric conditions.

We consider condensation and evaporation of the aerosol particles covered by liquid water. We take 80 discrete size classes, logarithmically distributed from $r_{\min}=80$ nm to $r_{\max}=10$ μm. The log-normal distribution of particles is

$$f=\frac{N_t}{(8\pi)^{1/2}r\rho\ln\sigma_g}\exp\left[-\frac{\ln(2r)-\ln(2r_m)}{2\ln^2\sigma_g}\right]^2, \tag{15}$$

where $N_t=\rho\int fdr=10^3\ \mathrm{cm^{-3}}$ is the total number of particles, $r_m=1.5$ μm, and $\sigma_g=1.1$.

Taking the supersaturation $S = p_v/p_0 - 1$ as a parameter, we recalculate the water mass fraction

$$Y_{H_2O} = \frac{m_v}{m}\frac{p_0}{p}(S+1), \tag{16}$$

where p_0 is water vapor pressure over a flat surface (see Table 1). We assume that the air consists of a mixture of oxygen (O_2), nitrogen (N_2) and water vapor (H_2O). The oxygen mass fraction (see Eq. (4)) is taken to be $Y_{O_2} = 26\%$, while the nitrogen mass fraction is obtained from the condition of normalization $Y_{N_2} = 1 - Y_{O_2} - Y_{H_2O}$. Since Y_{H_2O} depends on air molar mass m, and m itself depends on Y_{H_2O}, to find Y_{H_2O} we use iterations.

We take the following initial distribution of temperature in x-direction:

$$T(x) = \frac{T_2+T_1}{2} + \frac{T_2-T_1}{2}\frac{[\exp(x/\delta_x) - \exp(-x/\delta_x)]}{[\exp(x/\delta_x) + \exp(-x/\delta_x)]}, \tag{17}$$

where temperature $T_1 = 290$ K and supersaturation $S_1 = 0$ % are the values on the left boundary ($x = -220$ cm), and temperature $T_2 = 290$ K and supersaturation $S_2 = 0.5$ % are on the right boundary ($x = 280$ cm). The initial thickness of the cloud edge is $\delta_x = 100$ cm. Values of temperature and supersaturation determine water vapor mass fractions, $Y^1_{H_2O}$ and $Y^2_{H_2O}$ on the left and right boundaries, respectively. The initial x-profile for water vapor is

$$Y_{H_2O}(x) = \frac{Y^1_{H_2O} + Y^2_{H_2O}}{2} + \frac{Y^2_{H_2O} - Y^1_{H_2O}}{2}\frac{[\exp(x/\delta_x) - \exp(-x/\delta_x)]}{[\exp(x/\delta_x) + \exp(-x/\delta_x)]}. \tag{18}$$

The initial temperature and water vapor profiles are shown in Fig. 1 by the dashed curve.

The pressure $p = 1$ atm is the same everywhere, and the density is calculated using the equation of state (7). For example, if the temperature is taken to be $T = 293$ K then the density is $\rho = 1.2 \times 10^{-3}$ g cm^{-3}. Initially the x-component of velocity is assumed to be constant everywhere in the domain, $\boldsymbol{U}_x = 30$ cm/s. The particle distribution is taken to be the same everywhere in the domain, and at boundaries we use symmetric boundary conditions (The PENCIL Code, 2001). A summary of the boundary conditions is presented in Table 2.

3. Results

3.1. One-dimensional model

For the test purpose we start with a one-dimensional model. Also, the 1D approach allows us to study the complicated air–aerosol system in a laminar regime. For simplicity, buoyancy is ignored here. We take the size of the domain as 500 cm and 512 grid points. Fig. 1 shows the temperature, supersaturation and distribution of particles at times $t = 0$ s, 1 s and 2 s. Analyzing the distribution of particles with different sizes we find that the largest particles accumulate inside the front (or cloud edge), while the maximal concentration of smaller particles is before and after it. The maximum of S is inside the front, and therefore,

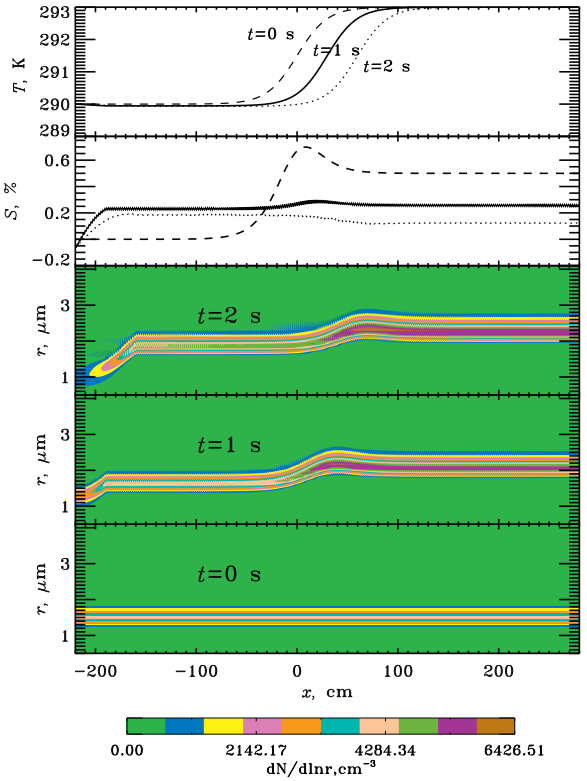

Fig. 1. Distributions of temperature T, supersaturation S and contour plots of particle concentration as a function of x-coordinate and particle size at $t = 0$ s (dashed curve), 1 s (solid curve), and 2 s (dotted curve).

the most intensive growth of particles due to condensation of water happens there. Moreover, the smaller the particles the larger is the growth rate (see Eq. (9)). Thus, at every time step the largest particles appear inside the front, while the smaller particles are accumulated before the front and after it. Since supersaturation is positive behind the front, the particles activate there.

Also, one can see that the size of droplets located between -250 cm to -50 cm is increasing in time, while the initial supersaturation in this area is zero. Initially this area is in non-stable equilibrium. When the calculation starts, the temperature first increases a bit because of the viscous term (the Smagorinsky model is still included even in a laminar case). Then supersaturation becomes a bit smaller than zero and small particles start to evaporate. Because of evaporation, water

Table 2
Boundary conditions at $x = -220$ cm and $x = 280$ cm; s – symmetric and a – antisymmetric (see details in The PENCIL Code (2001)).

	$x = -220$ cm	$x = 280$ cm
T	290 K	293 K
$\boldsymbol{U}_x$	30 cm/s	a
ρ	s	s
Y_{O_2}	26%	26%
Y_{H_2O}	$S = 0$ %	s
Y_{N_2}	Normalization	Normalization

pressure increases. Since large particles are still activating, the temperature does not increase much. Supersaturation is growing and becomes positive, leading to activation of all particles. This happens for the first 0.1–0.2 s, after that all particles are activating and the temperature is decreasing.

We also studied the structure and evolution of the cloud edge for different front thicknesses, inlet velocities, and parameters S and $B(r_0)$, and did not find any new features. Based on these test cases, we conclude that the presented cloud droplet module works correctly and we can continue with multidimensional simulations.

3.2. Multidimensional model setup

Now we consider a 3D domain of the size 500 cm × 250 cm × 250 cm. The direction of buoyancy force coincides with y-axis. In y- and z-directions we take periodic boundary conditions for all variables. The initial x-velocity component $\boldsymbol{U}_x$ is taken to be

$$\boldsymbol{U}_x(x,y,z) = 30 \text{ cm/s} \times \cos\left(\pi \frac{y}{Ly}\right), \tag{19}$$

where $Ly = 280$ cm is the vertical size of the domain. The same $\boldsymbol{U}_x$ velocity profile is used as boundary condition at $x = -220$ cm. In the right hand side part of the domain, there is a vertical motion, and the horizontal flux interacts with it near $x = 0$, i.e. $\boldsymbol{U}_y(x \geq 0) = 100$ cm/s (Siebesma et al., 2003; Flossmann and Wobrock, 2010; Boy et al., 2011). The initial $\boldsymbol{U}_y(x < 0)$ and $\boldsymbol{U}_z$ are taken to be zero. All other initial and boundary conditions are the same as in Section 2.4. The structure of the motion is shown in Fig. 2 (left upper corners).

To study the effect of turbulence on aerosol dynamics at the beginning of the simulations, we generate isotropic turbulence: the first iterations (during the first 10^{-3} s) are made without aerosol dynamics, but with randomly directed external forces (The PENCIL Code, 2001). After 10^{-3} s the external forces are set to zero, and the aerosol particles start to evolve. The time step of integration is 10^{-6} s.

3.3. Analysis of particle activation for 2D and 3D models with different grid cell sizes

One of the purposes of this paper is to check how crucial the Smagorinsky approximation is for the calculation of activation/evaporation of aerosol particles. The smaller the cell size, the closer it is to the Kolmogorov scale, and therefore the descriptions of turbulence, TKE dissipation, and air temperature are closer to the reality. Whereas for cell sizes larger than the Kolmogorov scale, one should describe the subgrid scale turbulence with a corresponding model (in our case the Smagorinsky model); therefore, the air temperature appears to be different from the correct one because of the corresponding approximations. This can be crucial for the final particle distribution.

Additionally, since the full 3D simulations are computationally extremely demanding, we will test whether a 2D model is appropriate for correct description of aerosol dynamics. For this task we compare the results of 2D and 3D simulations with the same settings but with different grid sizes. For two-dimensional simulations we use cell sizes of 4 cm, 2 cm, 1 cm and 0.5 cm, and for three-dimensional simulations sizes of 4 cm, 2 cm and 1 cm. Note that the estimated Kolmogorov scale is about 1 mm.

Fig. 3 shows the number of the particles N_{act} with the radius larger than 3 μm as a function of time (here and further we name such particles "activated particles"), i.e.

$$N_{\text{act}} = \int_V \rho \int_{r_0}^{r_{\max}} f dr, \tag{20}$$

where V is the volume of the domain and $r_0 = 3$ μm.

Let us first compare the results of 2D and 3D simulations for cell sizes of 4 cm (blue dotted curve and blue diamonds), 2 cm (green dashed curve and green triangles), 1 cm (red dotted-dashed curve and red asterisks), and 0.5 cm (black solid curve). Next, for simplicity, we name the case of 4 cm cell size as *case 1*, the 2 cm cell size as *case 2*, the 1 cm cell size as *case 3* and the

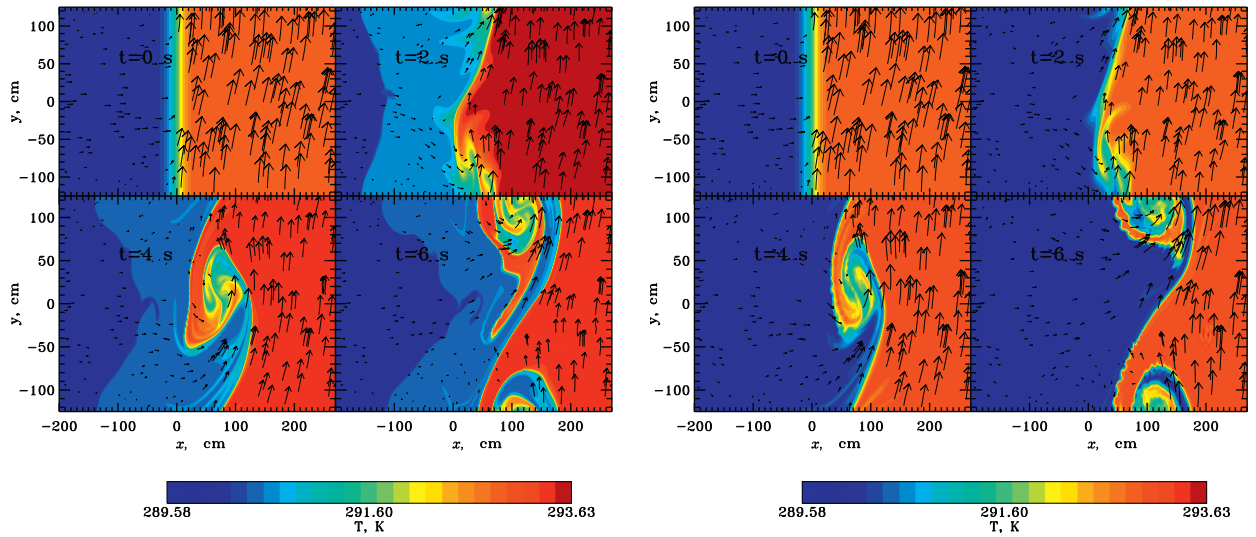

Fig. 2. Velocity (shown by arrows) and temperature fields in the 2D calculated domain for grid cell sizes of 0.5 cm (left panel) and of 2 cm (right panel) at $t = 0, 2, 4$, and 6 s.

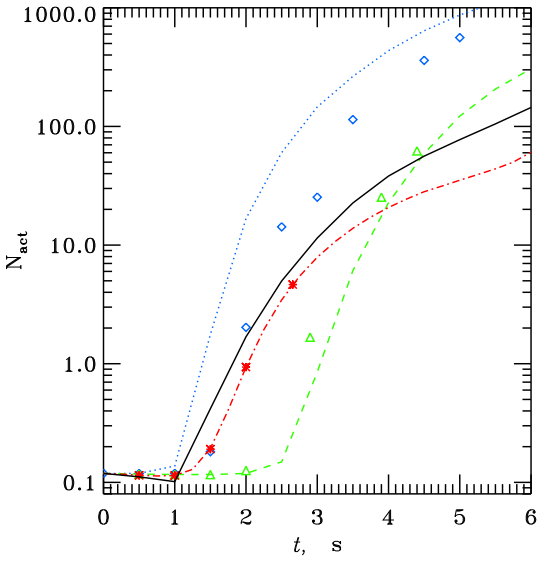

Fig. 3. Number of activated particles (with the size larger than 3 μm) averaged over the whole simulation domain, N_{act}, as a function of t for 2D model runs with grid cell sizes of 4 cm (blue dotted curve), 2 cm (green dashed curve), 1 cm (red dotted-dashed curve) and 0.5 cm (black solid curve) and for 3D model runs with grid cell sizes of 4 cm (blue diamonds), 2 cm (green triangles) and 1 cm (red asterisks). (For interpretation of the references to color in this figure legend, the reader is referred to the web version of this article.)

0.5 cm cell size as *case 4* (see Table 3). We see that for the first second almost all particles stay non-activated in all considered cases both for 2D and 3D simulations. Next for $t > 1$ s, particles start to activate in *cases 1*, *3*, and *4*, and the most intensive growth of particles happens in the case with the lowest resolution, *case 1*. Note that in *case 2*, the intensive activation occurs only after 2 s, whereas the activation rate is comparable with that in *case 1*. In *cases 3* and *4*, the activation rates are comparable, and they are smaller than the corresponding rates in *cases 1* and *2*. At $t > 4$ s, a number of activated particles become larger in *case 1* and *case 2* than in *case 3* and *case 4*, and the difference continues to increase with time. In Fig. 3 one can see a nonlinear behavior of the curves depending on the grid cell size.

Based on this analysis we conclude that the 3D simulations with a resolution of 1 cm (red asterisks in Fig. 3) have the most realistic results. If we now look at both the 3D simulation with the next higher resolution of 2 cm and the 2D simulation with the same resolution of 1 cm we see a higher agreement with the 2D runs. Thus, we believe that the results of 2D and 3D simulations differ much less than the results of 3D simulations with different cell sizes. We conclude that for studying the particle activation a 2D model is appropriate, and therefore, 2D simulations with high resolution give more realistic results than a 3D simulation with a lower resolution. This decreases the computer resources needed for studying the aerosol dynamics and provides the possibility to carry out more numerical experiments for more detailed understanding of the cloud edge structure.

Table 3
Summary of multidimensional runs (the curves are used in Fig. 3).

Resolution	2D model	3D model
4 cm (*case 1*)	Blue dotted	Blue diamonds
2 cm (*case 2*)	Green dashed	Green triangles
1 cm (*case 3*)	Red dotted-dashed	Red asterisks
0.5 cm (*case 4*)	Black solid	–

3.4. 2D simulations for grid cell sizes of 2 cm and 0.5 cm

Now we analyze the results of 2D simulations in *case 2* and *case 4*. Fig. 4 shows the supersaturation S at $t = 0$ s, 2 s, 4 s and 6 s. The results show a substantial difference in the distributions. In *case 4* the supersaturation is much smaller both before and behind the cloud edge than in *case 2*. Note that this is an area of the most intensive mixing. Only near the left boundary of the domain the supersaturation is almost the same in both cases. The reason for this is in the temperature difference (see Fig. 2). In the case of higher air temperature the supersaturation appears to be smaller (see Eq. (16)). The difference in temperature distributions is not large (smaller than 1°), but it appears to be important for supersaturation, and therefore for particle distribution (see details in the next paragraph). To interpret this fact in Fig. 5 we present the total air mass M in the area of the most intensive mixing [−100 cm, 200 cm] as a function of time (M_0 is the total mass at $t = 0$ s). One can see that for the first second the mass in this area is increasing faster in the higher resolution cases. Thus, in the case of resolved microturbulence (*case 4*), at the first second the air is adiabatically contracted and therefore heated more efficiently. We also checked the effect of viscous dissipation and found that viscous heating is much smaller than adiabatic heating.

In Fig. 6 we compare the number of activated particles

$$n_{act} = \rho \int_{r_0}^{r_{max}} f dr, \tag{21}$$

for *case 2* and *case 4* at $t = 1$ s, 2 s, 4 s, and 6 s, and also find crucial differences. Note that since in our model the total number of particles is not conserved with time, there is no sense to compare these two cases quantitatively. However, qualitative analysis of such distributions can be done. In *case 2* the particles are most effectively activated near the cloud edge (mostly before the edge), and the size of this area increases with time. In *case 4* the particles more intensively activate in the flux near the left boundary, where the turbulence is weak (we assume that the incoming flux is laminar). On the other hand, near the cloud edge the motion is strongly turbulent, and here a small amount of activated particles exists. In other words, we conclude that in *case 4* the stronger the turbulence, the weaker the activation of particles, whereas in *case 2* it is vice versa. This result confirms that the resolution of the computational domain is extremely important for the correct description of aerosol dynamics.

Finally, we average the particle distribution function in y-direction and compare the y-averaged number of particles with corresponding size as a function of x-coordinate for *cases 2* and *4* in Fig. 7. One can see that, for example at $t = 4$ s in *case 4* almost all small particles behind the edge evaporated, while in *case 2* there is a peak of the particle distribution function near

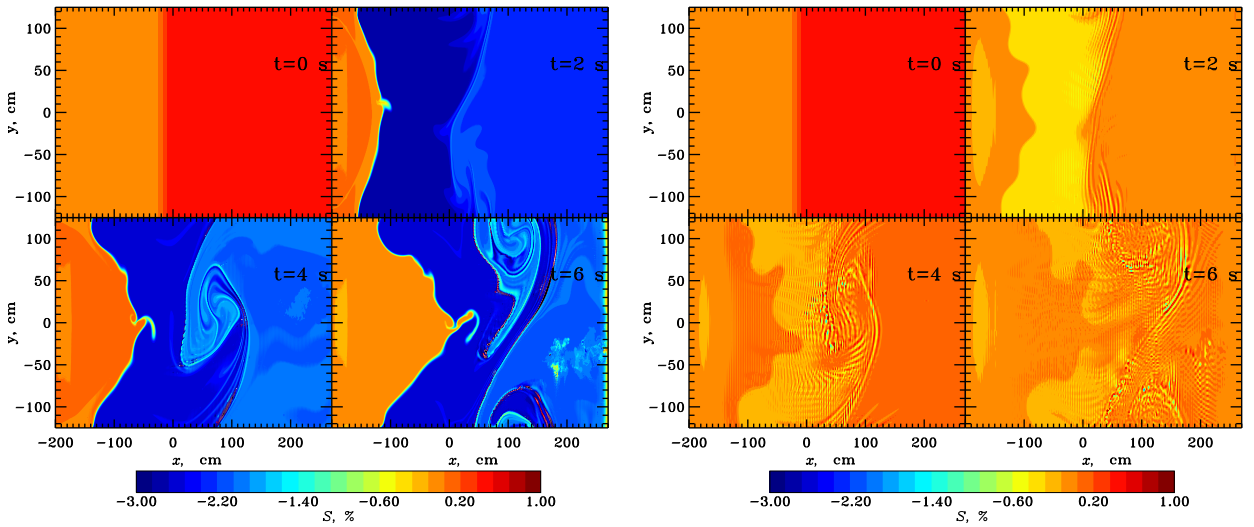

Fig. 4. 2D distributions of supersaturation S for grid cell sizes of 0.5 cm (left panel) and 2 cm (right panel) at $t = 0, 2, 4$, and 6 s. Left hand side of the distribution at $t = 0$ s corresponds to $S = 0$ %.

1 μm. Comparing the temperature behind the cloud edge for *cases 2* and *4* (see Fig. 2) we find that the air is warmer in *case 4* and the temperature difference is about 0.5 K. One of the reasons for this difference is the presence of microturbulence (in *case 4*). While the temperature difference is quite small, it appears to be crucial for the supersaturation because of the exponential dependence of supersaturation on the air temperature. In Fig. 4 we see that in *case 4* the supersaturation is negative in most parts of the domain, and its minimal value is −3%, while in *case 2* the supersaturation is positive almost everywhere in the domain. Thus, in *case 4* all small particles evaporated and only large particles survive because their lifetime is larger than the simulation time. Moreover, large particles capture the released water vapor molecules and continue growing (see Fig. 7, left panel). In *case 2* there is no such intensive evaporation ($S \geq 0$) and small particles can survive. This result also shows how the microturbulence is important for the aerosol dynamics in the atmosphere.

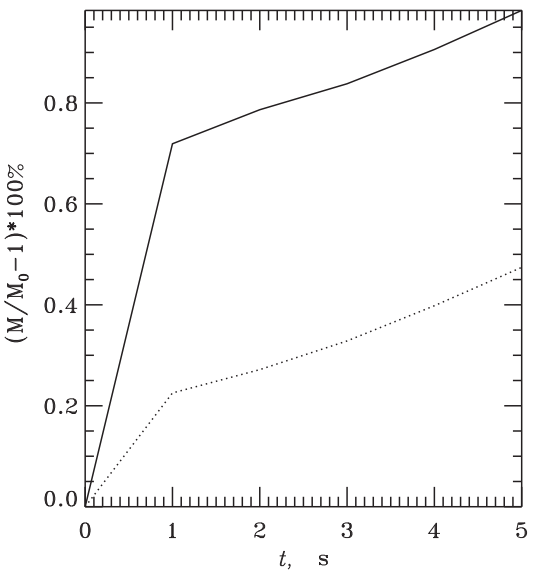

Fig. 5. A ratio of the total air mass in the domain M to the total mass M_0 at $t =$ 0 s as a function of time. Solid curve is the case of 0.5 cm grid cell size and dotted curve is the case of 2 cm grid cell size.

3.5. Effect of turbulent motion on aerosol dynamics

Now we inspect the influence of turbulent motion on aerosol dynamics, and vice versa. First, we study the effect of aerosol dynamics on the air temperature. Fig. 8 shows the temperature difference between the results with aerosol and without it. Analyzing simultaneously the temperature distribution in Fig. 2 and temperature difference in Fig. 8, we conclude that the activation of particles increases the air temperature by about 0.03 K, and the evaporation of particles decreases the temperature by about 0.26 K.

Also, we study the area of the most intensive mixing (note that this is the area of the cloud edge itself). Fig. 9 shows the difference in supersaturation $(S - S_a)/|S_a|$ for 2D runs (at $t = 4$ s) without aerosol dynamics, S_a, and with including it, S. We can see that aerosol dynamics increases the supersaturation in the most part of the domain by 16%, and in some places by up to 46%.

Analyzing the results of multi-dimensional simulations we found large numerical wiggles in the low resolution case for $t \gtrsim 2$ s (see Figs. 4, 7, right panel). Also, small wiggles appear in the high resolution case (see Figs. 8, 9). Trying different resolutions and thicknesses of the cloud edge we found two possible reasons for numerical wiggles: (i) aerosol dynamical processes that require shorter time step that we have used and (ii) not sufficiently high (or low) resolution of turbulence simulations (these two coupled). Indeed, fringes can appear in particle distribution nearby the smallest particles because of the too long time step. For example, to move 100 nm particles from one bin to another the time step should be about 10^{-7} s, but the larger the particles the larger time step can be used ($dt \sim r^2$). For our simulations we take the maximum of the

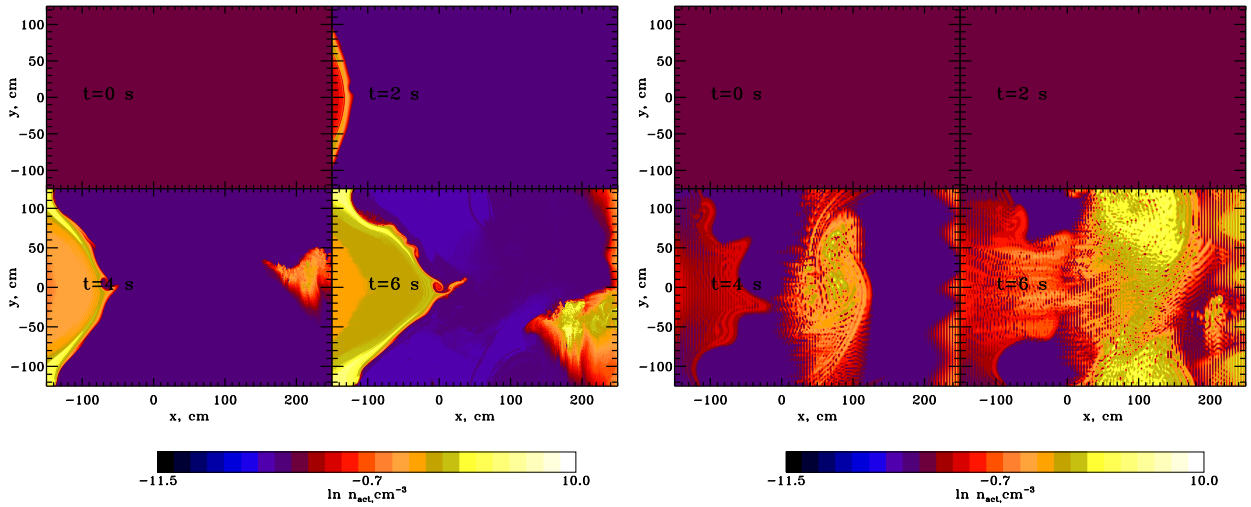

Fig. 6. Distribution of activated particles, n_{act}, for grid cell sizes of 0.5 cm (left panel) and 2 cm (right panel) at $t = 0, 2, 4$, and 6 s.

initial distribution near 10 μm and the time step of about 10^{-6} s. Even with such time step the simulations are very computationally demanded. Also, we found that the wiggles appear because the fine scale turbulence is not sufficiently resolved. This fine scale turbulence develops and is more pronounced at times larger than 2 s, and it is more evident when the resolution is lower. Note, that at $t = 2$ s in the case of 0.5 cm resolution there are no wiggles, but in the case of 2 cm resolution small wiggles already appear. Therefore, the high resolution case represents more correctly turbulence structure and resulting aerosol dynamics compared to the lower resolution case.

4. Conclusions

In this paper we study the aerosol activation process at a cloud edge. We consider the flux of aerosol particles, through the boundary between dry and moist air. We take into account the condensation and evaporation of the aerosol particles covered by liquid water, and assume initially a lognormal distribution.

For the test purpose we start with a one dimensional problem to study the motion and evolution of the front between the areas of dry air and moist air. A flux of dry air with 10^3 aerosol particles per cm^3, with the maximum of

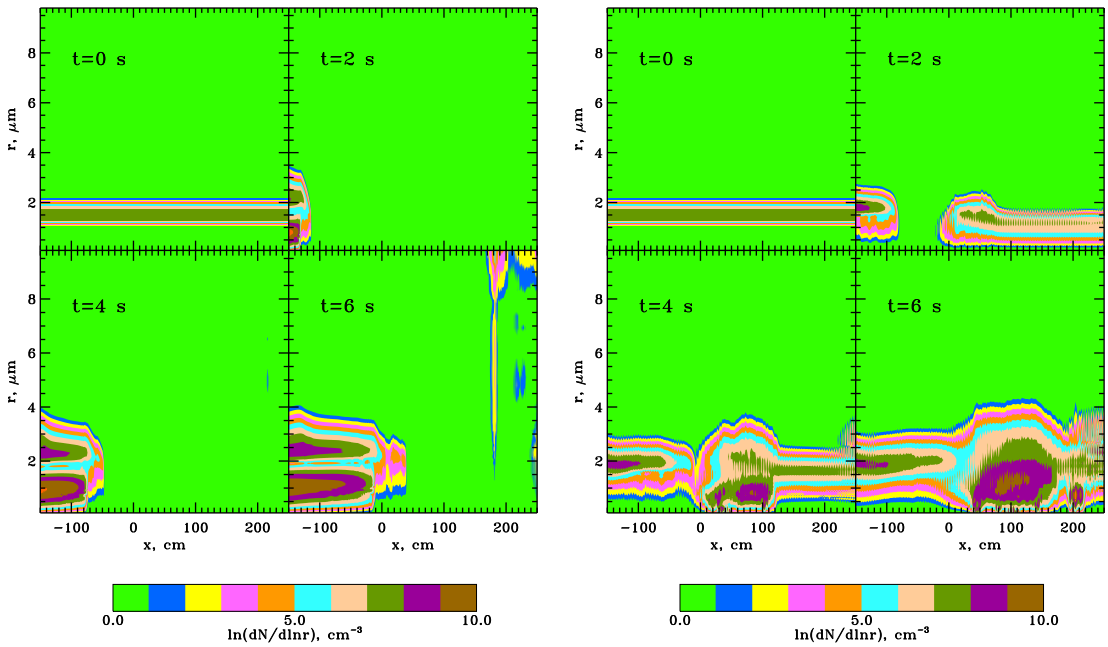

Fig. 7. Contour plots of particle concentration averaged in y-direction for grid cell sizes of 0.5 cm (left panel) and 2 cm (right panel) at $t = 0, 2, 4$, and 6 s.

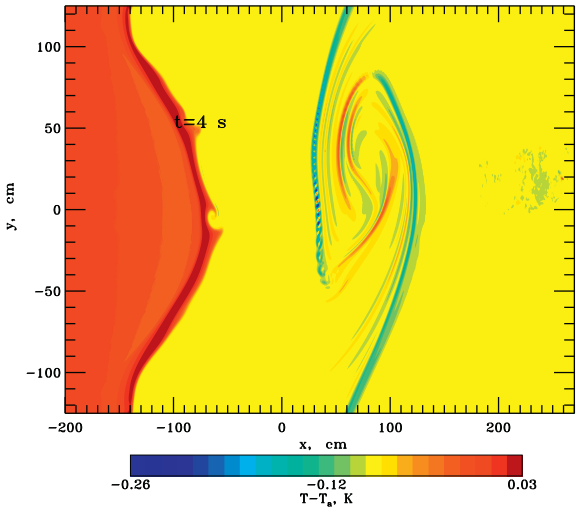

Fig. 8. Contour plot of the difference between air temperatures in the 2D model with and without included aerosol dynamics. The grid cell size is 0.5 cm.

distribution at $r_m = 1.5$ μm and supersaturation $S = 0$ %, is coming into the domain with inlet velocity $\boldsymbol{U}_{in} = 30$ cm/s and interacts with a wet cloud edge. The supersaturation behind the front is $S = 0.5$ %. This approach allows us to analyze the

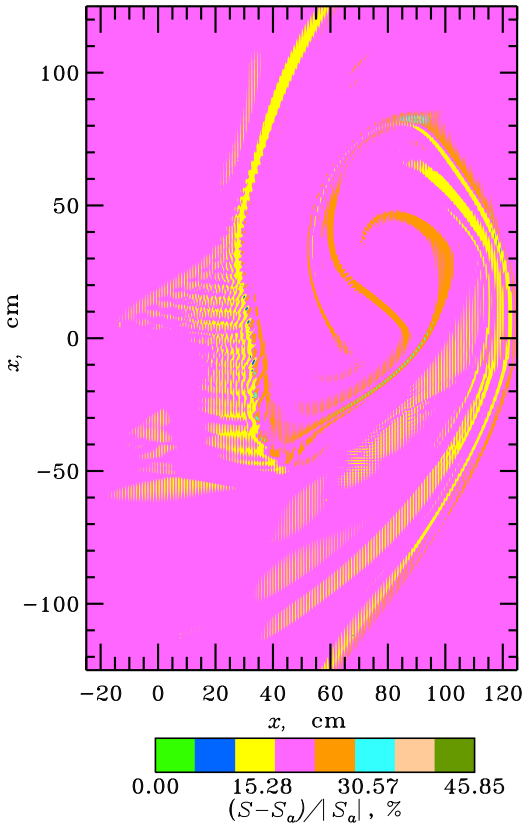

Fig. 9. Contour plot for the difference between the supersaturation, $(S - S_a)/|S_a|$ for the 2D model at $t = 4$ s with aerosol dynamics, S, and without it, S_a. The grid cell size is 0.5 cm.

effect of the fluid mechanics on the aerosol dynamics (and vice versa) in a laminar regime. Using a 1D approach we find that the most intensive growth occurs inside the front, i.e. the distribution of the largest particles has a maximum there. Then this single maximum splits into two maxima, and they shift toward the front edges. In other words, at every time step the largest particles are located in the front, and the smaller particles are accumulated before and after it.

Next, we make 2D and 3D simulations with a more complicated velocity field at the cloud edge. We assume that the dry air flux is coming into the computational domain in the middle part and going out near the boundaries. Moist air moves in horizontal direction with velocity $\boldsymbol{U}_y = 100$ cm/s. The third velocity component is initially zero, $\boldsymbol{U}_z = 0$ cm/s. Initial conditions are the same as in the 1D case. After several seconds the cloud edge forms a curved shape and we analyze the final distributions of the aerosol particles.

Since the Kolmogorov scale is much smaller than the typical grid cell size of numerical simulation in atmospheric science ($O(1)$ mm), we use the Smagorinsky model for the subgrid scale turbulence. To analyze the validity of the Smagorinsky approximation for the description of turbulent motion of air with aerosol particles, we compare the number of activated particles in 2D and 3D models with different resolutions (4 cm, 2 cm, 1 cm and 0.5 cm grid cell sizes). We find that the differences between the results of 2D simulations with different grid cell sizes are much larger than those between 2D and 3D simulations with the same cell size. Therefore, we conclude that a high resolution 2D model gives more realistic results for the simulations of activated particles than a similar 3D model with lower resolution.

Next, we compare the results of 2D simulations for grid sizes of 2 cm and 0.5 cm. We analyze the distributions of supersaturation and the concentration of activated particles in the domain at times $t = 0$ s, 1 s, 2 s, and 4 s. We show that the small scale turbulence plays an important role in particle activation. In a high resolution case, activation is limited at the cloud edge (meaning no activation in the middle of the domain, occurring mainly at the domain boundaries in x-direction), whereas this is opposite in a case of lower resolution.

Finally, we investigate the interactions between turbulence and microphysics. We find that aerosol dynamics increases the supersaturation in most parts of the domain by 16%, and in some places even by 46%. Activation of particles decreases the air temperature by about 0.03 K, and evaporation increases it by about 0.26 K.

We should note that in this study the initial and boundary conditions are taken as typical parameters for the atmospheric conditions. Next we are planning to use the results of an LES simulation for a more detailed description of the boundaries. Also, size distribution for the aerosol core and a more detailed chemistry will be added in the future.

Acknowledgments

This work was financially supported by the Helsinki University Centre for Environment (HENVI, 251427), and the Academy of Finland (139656). Computational resources from CSC — IT Center for Science Ltd. are all gratefully acknowledged.

References

Andrejczuk, M., Grabowski, W., Malinowski, S., Smolarkiewicz, P., 2004. Numerical simulations of cloud—clear air interfacial mixing. J. Atmos. Sci. 61, 1726–1739.

Andrejczuk, M., Grabowski, W., Malinowski, S., Smolarkiewicz, P., 2006. Numerical simulations of cloud–clear air interfacial mixing: effects on cloud microphysics. J. Atmos. Sci. 63, 3204–3225.

Andrejczuk, M., Grabowski, W., Malinowski, S., Smolarkiewicz, P., 2009. Numerical simulation of cloud–clear Air interfacial mixing: homogeneous versus inhomogeneous mixing. J. Atmos. Sci. 66, 2493–2499.

Babkovskaia, N., Haugen, N., Brandenburg, A., 2011. A high-order public domain code for direct numerical simulations of turbulent combustion. J. Comput. Phys. 230, 1–12.

Boy, M., Sogachev, A., Lauros, J., Zhou, L., Guenther, A., Smolander, S., 2011. SOSA — a new model to simulate the concentration of organic vapours and sulphuric acid inside the ABL. Atmos. Chem. Phys. 1, 43–51.

Brenguier, J.-L., Grabowski, W.W., 1993. Cumulus entrainment and cloud droplet spectra: a numerical model within a two-dimensional dynamical framework. J. Atmos. Sci. 50, 120–136.

Dobler, W., Stix, M., Brandenburg, A., 2006. Magnetic field generation in fully convective rotating spheres. Astrophys. J. 638, 336–343.

Flossmann, A., Wobrock, W., 2010. A review of our understanding of the aerosol-cloud interaction from the perspective of a bin resolved cloud scale modelling. Atmos. Res. 97, 478–497.

Haugen, N.E., Brandenburg, A., 2006. Hydrodynamic and hydromagnetic energy spectra from large eddy simulations. Phys. Fluids 18, 1–7.

Hirschfelder, J., Curtiss, J., Byrd, B., 1969. Molecular Theory of Gases and Liquids. John Wiley & Sons, New York.

Kumar, B., Schumacher, J., Shaw, R.A., 2013. Cloud microphysical effects of turbulent mixing and entrainment. Theor. Comput. Fluid Dyn. 27 (3), 361–376.

Lanotte, A.S., Seminara, A., Toschi, F., 2009. Cloud droplet growth by condensation in homogeneous isotropic turbulence. J. Atmos. Sci. 66 (1685–1697).

Makkonen, R., Asmi, A., Kerminen, V.-M., Boy, M., Arneth, A., Hari, P., Kulmala, M., 2012. Air pollution control and decreasing new particle formation lead to strong climate warming. J. Atmos. Chem. Phys. 12, 1515–1524.

Mattila, T., Kulmala, M., Vesala, T., 1997. On the condensational growth of multicomponent droplet. J. Aerosol Sci. 28, 553–564.

Mellado, J.P., 2010. The evaporatively driven cloud-top mixing layer. J. Fluid Mech. 660, 5–36.

Morales, R., Nenes, A., Jonsson, H., Flagan, R.C., Seinfeld, J.H., 2011. Evaluation of an entraining droplet activation parameterization using in situ cloud data. J. Geophys. Res. 116, D15205.

Romakkaniemi, S., McFiggans, G., Bower, K.N., Brown, P., Coe, H., Choularton, T.W., 2009. A comparison between trajectory ensemble and adiabatic parcel modeled cloud properties and evaluation against airborne measurements. J. Geophys. Res. 114, D06214.

Seinfeld, J.H., Pandis, S.N., 2006. Atmospheric Chemistry and Physics: From Air Pollution to Climate Change. John Wiley & Sons Inc.

Siebesma, A., Bretherton, C., Brown, A., Chlond, A., Cuxart, J., Duynkerke, P., Jiang, H., Khairoutdinov, M., Lewellen, D., Moeng, C.-H., Sanchez, E., Stevens, B., Stevens, D., 2003. A large eddy simulation intercomparison study of shallow cumulus convection. J. Atmos. Sci. 60, 1201–1215.

Slawinska, J., Grabowski, W., Pawlowska, H., Morrison, H., 2012. Droplet activation and mixing in large-eddy simulation of a shallow cumulus field. J. Atmos. Sci. 69, 444–462.

The PENCIL Code, 2001. http://pencil-code.googlecode.com.

Twomey, S., 1977. The influence of pollution on the shortwave albedo of clouds. J. Atmos. Sci. 34, 1149–1152.

Wood, R., Irons, S., Jonas, P.R., 2002. How important is the spectral ripening effect in stratiform boundary layer clouds? Studies using simple trajectory analysis. J. Atmos. Sci. 59, 2681–2693.

Wyszogrodzki, A., Grabowski, W., Wang, L.-P., 2011. Activation of cloud droplets in bin-microphysics simulation of shallow convection. Acta Geophys. 59 (6), 1168–1183.